Single-particle dynamics of liquid CCl_4: a comparison of molecular dynamics and neutron quasi-elastic scattering results

1992 J. Phys.: Condens. Matter 4 1213

(http://iopscience.iop.org/0953-8984/4/5/002)

J. Phys.: Condens. Matter 4 (1992) 1213–1231. Printed in the UK

Single-particle dynamics of liquid CCl_4: a comparison of molecular dynamics and neutron quasi-elastic scattering results

A Chahid†, F J Bermejo†, E Enciso‡, M Garcia Hernandez† and J L Martinez§

† Consejo Superior de Investigaciones Cientificas (CSIC), Instituto de Estructura de la Materia, Serrano 123, E-28006, Madrid, Spain

‡ Departamento Quimica-Fisica, Universidad Complutense de Madrid, E-28040 Madrid, Spain

§ Institut Laue–Langevin, 156X, F-38042 Grenoble Cédex, France

Received 25 July 1991, in final form 19 September 1991

Abstract. The molecular translation and rotational motions of liquid CCl_4 are studied by means of the concurrent use of computer molecular dynamics simulations as well as neutron quasi-elastic scattering. The relevant correlation functions have been analysed in terms of simple analytical models and the total spectra are compared with the measured ones. The data confirms the substantial departure from simple rotational or diffusion behaviour encountered in a previous work.

1. Introduction

Liquid carbon tetrachloride is considered to be perhaps the simplest molecular liquid due to its high molecular symmetry and to the fact that the interparticle potential can be reasonably well represented in terms of a sum of pair interactions with only a relatively small electrostatic contribution arising from the permanent molecular octupole moment. It can therefore be considered as a molecular analogue to liquefied rare gases, and it therefore constitutes a prime candidate to test the effects of the molecular shape on the microscopic dynamics.

The liquid structure has already been studied in detail [1] along with its microscopic dynamics at low [2] and high [3] energy transfers by neutron inelastic scattering.

The purpose of the present work is to explore the single-particle dynamics of such a simple molecular liquid. A recent quasi-elastic study has shown [2] a number of difficulties that appear when rather simplified physical models are used to analyse the spectra. In such a respect, both the linear and angular velocity correlation functions are analysed in detail, in order to compare the results with those arising from the fits to the quasi-elastic spectra. On the other hand, it extends the quasi-elastic experiments towards higher energy resolution. So that it allows the determination of the incoherent linewidth to be free of the complications caused by the need of isolating this component when larger energy windows are used.

0953-8984/92/051213 + 19 $04.50

The structure of the paper is as follows. A brief account of the relevant formulae connecting the experimental observables (neutron cross-sections) with the simulated quantities is presented in section 2. The description of the methods followed to compute the correlation functions is given in section 3. In section 4 some high resolution experimental data are presented and a discussion of the models used to analyse the simulated data is given in section 5. Finally, a summary and conclusions are presented in section 6.

2. Basic formulae

The partial differential cross-section $d^2\sigma/d\Omega\, d\omega$ of the scattering of an assembly of N identical molecules may be factored as a product of three quantities depending respectively on translations, rotations and vibrations, and following [4], it can be written as

$$\frac{d^2\sigma}{d\Omega\, d\omega} = \frac{N}{2\pi}\frac{k}{k_0}\int dt \exp(-i\omega t)\left[\left\{\sum_{\mu}(b^2_{\mu,\mathrm{inc}} + b^2_{\mu,\mathrm{coh}}(I_{\mu\mu}(Q,t) + \sum_{\mu\neq\nu} b_{\mu,\mathrm{coh}} b_{\nu,\mathrm{coh}} I_{\mu\nu}(Q,t)\right\} I_s(Q,t) + F(Q)(I(Q,t) - I_s(Q,t))\right]$$
$$= (k/k_0)S_{\mathrm{tot}}(Q,\omega) \tag{1}$$

where the $I(Q,t)$ functions comprise all the relevant microscopic dynamical information of the system and are divided into single-molecular ($I_{\mu\nu}(Q,t)$, $I_s(Q,t)$) and collective $I(Q,t)$ components.

$$I_{\mu\nu}(Q,t) = \langle \exp(iQ\cdot a_\mu(t))\exp(-iQ\cdot a_\nu(0))\rangle$$
$$I_s(Q,t) = (1/N)\sum_i \langle \exp(iQ\cdot R_i(t))\exp(-iQ\cdot R_i(0))\rangle \tag{2}$$
$$I(Q,t) = (1/N)\sum_{ij} \langle \exp(iQ\cdot R_i(t))\exp(-iQ\cdot R_j(0))\rangle$$
$$F(Q) = \left(\sum_\mu b_{\mu,\mathrm{coh}}\frac{\sin(Qa_\mu)}{Qa_\mu}\right)^2$$
$$b_{\mu,\mathrm{inc}} = \{\langle b_\mu^2\rangle - \langle b_\mu\rangle^2\}^{1/2}$$
$$b_{\mu,\mathrm{coh}} = \langle b_\mu\rangle$$

k_0 and k denote the incident and scattered neutron wavevectors, respectively; $Q = k - k_0$, $\hbar\omega = \hbar^2/2m(k^2 - k_0^2)$. b^i_μ denotes the bound scattering amplitude of the μth nucleus in the ith molecule. A similar meaning applies to b^j_ν. The bracket $\langle\ \rangle$ denotes an ensemble average and the sum over μ and ν runs over all the nuclei in the molecule, and those over i and j over all the molecules in the system. The position vector of the scattering nucleus was separated into three components, according to:

$$r^i_\mu(t) = R + a^i_\mu + u^i_\mu \tag{3}$$

where u^i_μ is the displacement of the nucleus μ from its equilibrium position within the molecule i, originating from internal vibrations, i.e. deformations of bond lengths and

angles, $\boldsymbol{R}_i$ denotes the position of the centre of mass (CM) and corresponds to the translational component, $\boldsymbol{a}_\mu^i$ is the rotational component and denotes the equilibrium position of the nucleus with respect to the CM.

The total cross-section (1) can also be written as a sum of quasi-elastic and inelastic contributions of both incoherent and coherent scattering. The quasi-elastic contribution can be written in terms of the scattering law $S(Q, \omega)$ as

$$S_{\text{tot}}^{\text{q-el}}(Q, \omega) = u^2(Q)S_{\text{inc}}(Q, \omega) + v^2(Q)S_{\text{coh}}(Q, \omega) \tag{4}$$

where $u(Q)$ and $v(Q)$ are molecular form factors given in terms of atom scattering lengths and distances to the centre of mass [2].

The rotational intermediate scattering function $I_{\mu\nu}(Q, t)$ can be written as an expansion in various partial waves each corresponding to a rotational angular momentum state 'l' of the CCl_4 molecule [5], i.e.

$$I_{\text{Cl,Cl}}(Q, t) = \sum_{l=0}^{\infty} (2l + 1)j_l^2(Qa_{\text{Cl}})F_l(t) \tag{5}$$

$$I_{\text{Cl,Cl}'}(Q, t) = \sum_{l=0}^{\infty} (2l + 1)j_l^2(Qa_{\text{Cl}})P_l(\cos\theta_{\text{Cl,Cl}'})F_l(t) \tag{6}$$

where j_l is the Bessel function of order l, P_l is the Legendre polynomial of order l, $\theta_{\text{Cl,Cl}'}$ is the angle between a pair of distinct Cl atoms [1] and $F_l(t)$ is a rotational relaxation function of order l. The subscript Cl, Cl refers to the same atom in the molecule whereas Cl, Cl' refers to a pair of atoms in the same molecule. Sears [5] has established the relation between these $F_l(t)$ functions and those introduced by Gordon, i.e.

$$F_l(t) = \langle P_l(\boldsymbol{u} \cdot \boldsymbol{u}(t))\rangle = \langle P_l(\cos\beta(t))\rangle \tag{7}$$

where β is the angle through which a vector $\boldsymbol{u}$ fixed in the molecule rotates in time t. All we know about $F_l(t)$ is that $F_0(t) = 1$ and that we may expect $F_l(t)$ for $l > 0$ to have a free rotator behaviour at small times and the characteristics of rotational diffusion at large times. Since $r_{\text{C-Cl}} = 1.7663$ Å [1], one immediately sees that for the range $0.2 < Q < 4$ Å^{-1} accessible to an instrument such as IN6 at the ILL [6] for example, one needs only to keep up to the $l = 2$ term in the expansion. So, in what follows, we restrict the calculation to $F_1(t)$ and $F_2(t)$, the most important rotational relaxation functions in cold neutron scattering experiments. $F_1(t) = \langle P_1(\cos\beta(t))\rangle$ is the single-molecule dipole autocorrelation function which can be obtained, for example, from a Fourier transform of an infra-red absorption spectrum. $F_2(t) = \langle P_2(\cos\beta(t))\rangle$ is related to the depolarized component of a rotational Raman band [7, 8].

3. Computational technique and results

3.1. Molecular dynamics simulation

Both translational and rotational equations of motion have been solved by applying the Gear predictor–corrector method [9]. The CM motions of molecules were followed using a fifth-order algorithm. Euler's equations of motion in quaternions were solved by a fourth-order algorithm, and 108 molecules were confined in a cubic box and subjected to periodic boundary conditions. Each run was started from a configuration from an equilibrated run at high temperature. In each computation the positions, the velocities,

Table 1. Parameters for the site–site potential.

Interaction	ε/k	σ(nm)
C–C	51.2	0.460
C–Cl	72.4	0.405
Cl–Cl	102.4	0.350

the quaternions and the angular velocities were stored every $\Delta t = 0.025$ ps in the high temperature thermodynamic state and $\Delta t = 0.020$ ps in the low temperature counterpart. The liquid densities were the ones corresponding to the experimental values at 293 and 260 K (1.66 and 1.58 g cm^{-3}), respectively. The intermolecular potential used is the site–site Lennard-Jones model proposed by McDonald *et al* [10]. Thus, the potential is

$$U(\boldsymbol{R}_{12}, \omega_1, \omega_2) = \Sigma U_{\alpha\beta}(r_{\alpha\beta}) \tag{8}$$

where $\boldsymbol{R}_{12}$ is the vector from the centre of molecule 1 to that of molecule 2, ω_i is the orientation of molecule i, $r_{\alpha\beta}$ is the distance between size α and a site β on molecule 2, and

$$U_{\alpha\beta}(r_{\alpha\beta}) = 4\varepsilon_{\alpha\beta}[(\sigma_{\alpha\beta}/r)^{12} - (\sigma_{\alpha\beta}/r)^{6}] \tag{9}$$

The relevant potential parameters are given in table 1. The potential used in the simulation was truncated with a site to site cut-off distance of one half of the box width.

The time-dependent correlations investigated here refer to quantities directly amenable to experimentation such as the single particle $I_s(Q, t)$ and the total $I(Q, t)$ intermediate scattering functions, as well as some others which, although not being directly observable with neutron scattering, specify the details of the molecular dynamics contained in the $I_{\mu\nu}(Q, t)$ functions. In particular, functions belonging to this latter class that will be computed are

the angular velocity autocorrelation function;
the first and the second rotational relaxation functions $F_1(t)$ and $F_2(t)$.

Other correlation functions not directly observable by neutron scattering will be also computed. These functions give information on the single particle dynamics and are:

the mean-square atomic displacement $\rho(t)$;
the velocity autocorrelation function $\psi(t)$.

3.2. The mean square displacement

$\rho(t)$ is calculated as follows:

$$\rho(\tau) = \langle |r(t) - r(0)|^2 \rangle = (1/N) \sum_{i=1}^{N} \frac{1}{\tau_{\max}} \sum_{\tau_0=1}^{\tau_{\max}} r_i(\tau + \tau_0) \cdot r_i(\tau_0) \tag{10}$$

where the first sum runs over the N molecules considered and the second sum runs over all the configurations (4726 configurations for $T = 260$ K and 3062 for $T = 293$ K). $r_i(t)$ is the position of the CM of the ith molecule. $\rho(t)$ is calculated with a time step of 0.2 ps

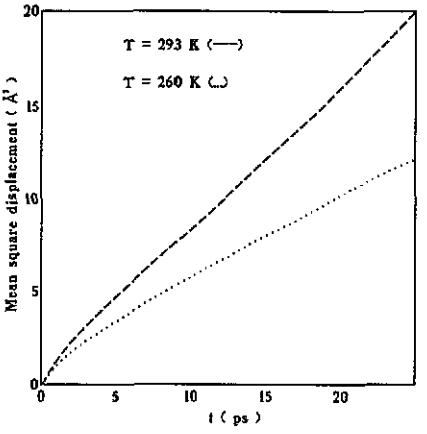

Figure 1. Mean square displacements $\langle r^2(t)\rangle$. The coefficients of the asymptotic form $6Dt + C$ are given by: $D = 0.450 \times 10^{-5}\,cm^2\,s^{-1}$ and $C = 1.5$ Å^2 for $T = 260$ K (dotted curve) and $D = 1.278 \times 10^{-5}\,cm^2\,s^{-1}$ and $C = 0.9$ Å^2 for $T = 293$ K (broken curve).

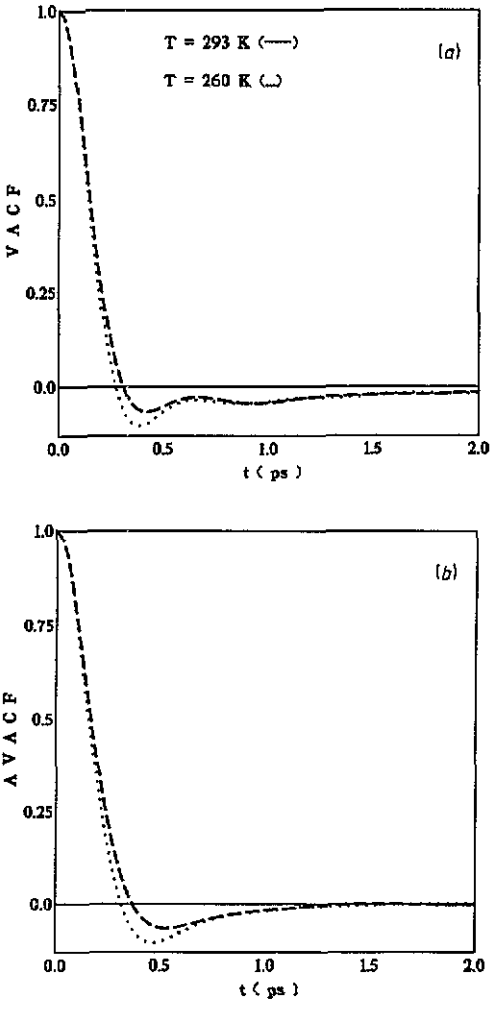

Figure 2. (*a*) Computed normalized velocity autocorrelation function (VACF) at time intervals of 0.02 ps and 0.025 ps respectively for $T = 260$ K (dotted curve) and $T = 293$ K (broken curve); (*b*) Computed normalized angular velocity autocorrelation function (AVACF) at time intervals of 0.02 ps and 0.025 ps respectively for $T = 260$ K (dotted curve) and $T = 293$ K (broken curve).

and is presented in figure 1. From this figure, it is seen that the asymptotic behaviour $6Dt + C$ of $\langle r^2\rangle$ is already achieved at about $t = 3$ ps.

3.3. Velocity autocorrelation function (VACF)

This function is the basic quantity in the discussion of self-diffusion. It is a measure of the projection of the particle velocity at time t onto its initial value, averaged over all

Table 2. Calculated values of D (in $10^{-5}\,cm^2\,s^{-1}$) and values obtained by experimental techniques.

	$D_s = 1/6t \lim \rho(t)$	D_i	Tracer diffusion	$D_{neutrons}$
$T = 260$ K	0.450	0.940	0.300	
$T = 275$ K				0.35
$T = 293$ K	1.278	1.695	1.284	

initial conditions. It is calculated as follows:

$$\psi(\tau) = \frac{\langle \boldsymbol{\nu}(t) \cdot \boldsymbol{\nu}(0) \rangle}{\langle \boldsymbol{\nu}(0) \cdot \boldsymbol{\nu}(0) \rangle} = \frac{1}{\nu_0^2} \frac{1}{N} \sum_{i=1}^{N} \frac{1}{\tau_{max}} \sum_{\tau_0=1}^{\tau_{max}} \boldsymbol{\nu}_i(\tau + \tau_0) \cdot \boldsymbol{\nu}_i(\tau_0). \tag{11}$$

Short time intervals are necessary for the calculation of the memory function of $\psi(t)$ so the VACF corresponding to $T = 260$ K and $T = 293$ K are computed at time intervals of 0.02 ps and 0.025 ps respectively. We show in figure 2(*a*) the normalized VACF for the two temperatures considered. This figure shows the general behaviour of this function, i.e. the very short-time behaviour $t < 0.1$ ps is seen to be insensitive to temperature and density variations. In this time region $\psi(t)$ is governed by the second frequency moment of its power spectrum $\psi(\omega)$; the intermediate time behaviour $0.1 < t < 0.5$ ps is seen to be quite sensitive to density and temperature. This behaviour evidences the presence of a large backscattering region where the negative value of $\psi(t)$ implies a high probability of a large angle deflection in the particle motion. In this respect it is radically different from the Langevin-type VACF, namely $\exp(-k_B T t/MD)$. The generalized frequency spectrum is given by:

$$\psi(\omega) = \frac{k_B T}{MD} \int \psi(t) \cos(\omega t)\, dt \tag{12}$$

and is shown in figure 3 for $T = 260$ K as well as the transform of a Langevin-type autocorrelation function which is included for comparison purposes.

As expected for $\psi(t)$, the so-called backscattering is weaker as T increases. The depth of the main minimum at 293 K is about one half the depth at 260 K.

The only transport coefficient we have determined is the diffusion coefficient. It has been computed either by the use of the Einstein relation, i.e. from the slope (D_s) of the linear part of the curve representing $\rho(t)$ or from the time integral (D_i) of the VACF, ie

$$D_i = \frac{k_B T}{M} \int \psi(t)\, dt. \tag{13}$$

Table 2 shows the computed values of D as well as the values obtained by tracer diffusion [11] and by neutrons (see section 4).

Both methods of calculation of the self-diffusion coefficient give different values which become more disparate as the temperature is lowered. Such a fact is caused by two types of errors. The first are caused by the difficulty of evaluating the integral in (13) since, in order to reduce the statistical noise, $\psi(t)$ is truncated at 5 ps. The main effect of such a truncation is the underestimation of long-time (hydrodynamic) tail of the

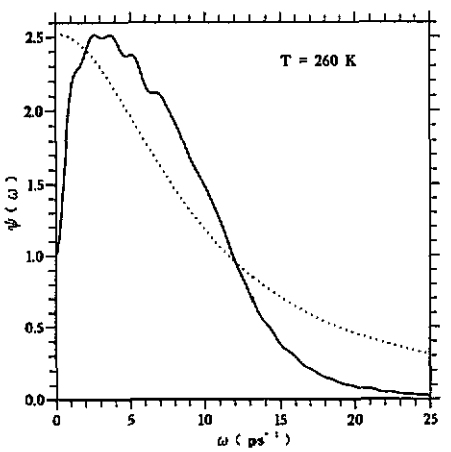

Figure 3. Spectrum of the VACF at $T = 260$ K (full curve) as well as the spectrum of the VACF of a Langevin type which is a Lorentzian (dotted curve).

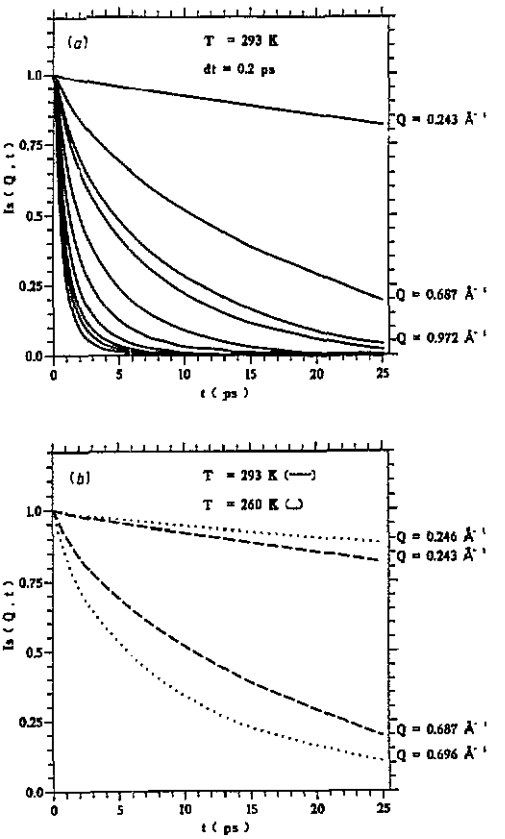

Figure 4. (*a*) Normalized incoherent scattering function $I_s(Q, t)$ at 293 K for several values of momentum transfers. These values are: 0.243, 0.687, 0.972, 1.059, 1.374, 1.683, 1.988, 2.226, 2.380 and 2.605 $Å^{-1}$. (*b*) Comparison of $I_s(Q, t)$ plotted for two different values of the triplet (n_1, n_2, n_3) at the two temperatures considered. This gives a momentum transfer of 0.246 and 0.696 $Å^{-1}$ for $T = 260$ K (dotted curve) and 0.243 and 0.687 $Å^{-1}$ for $T = 293$ K (broken curve).

autocorrelation function which at low temperatures has a noticeable oscillatory behaviour with a region below zero which extends until rather large times. The second type of errors comes from the fact that in a computer experiment it is not easy to construct an accurate ensemble average and then the calculation of the correlation function $\psi(t)$ is not accurate enough [12]. From arguments given in [13] the accuracy in the computed coefficients due to statistical averaging should not be better than 5%. On the other hand, in order to reconcile the disparate values of D computed using the two criteria, it would be necessary to perform a simulation with high-statistical accuracy at long times, something which was not attempted since our main focus of interest was to compare the simulation data with those obtained with QENS.

However, it can be seen that the agreement between the values calculated using the Einstein relation and those obtained by tracer diffusion or QENS is quite good, which

demonstrates that such a simplified procedure of estimation of D is accurate enough, at least for this class of non-associated liquids.

It is worth noting that the diffusion coefficient exhibits a dramatic change between the two temperatures (it is approximately double).

3.4. Intermediate scattering laws $I_s(Q, t)$ and $I(Q, t)$

The $I_s(Q, t)$ is computed as follows

$$I_s(Q, \tau) = (1/N) \sum_{i=1}^{N} (1/\tau_{max}) \sum_{\tau_0=1}^{\tau_{max}} (1/nt) \sum_{j=1}^{nt} \exp[iQ_j \cdot (r_i(\tau + \tau_0) - r_i(\tau_0))] \qquad (14)$$

where

$$Q_j = (2\pi/L)(n_{1j}, n_{2j}, n_{3j})$$

L is the length of the box; n_1, n_2, n_3 are integers and nt is the number of triplets (n_1, n_2, n_3) that gives the same module of Q.

The computation of $I_s(Q, t)$ is made at time intervals of 0.2 ps since it provides sufficiently good statistics. Figure 4(*a*) shows several constant Q plots of $I_s(Q, t)$ computed from data of the 293 K simulation. It is seen from this figure that the time dependence of $I_s(Q, t)$ is qualitatively the same in the explored Q range: a fast decay during the first picosecond which becomes more noticeable as Q increases, followed by a much slower decay at long times. The same is obtained for the 260 K simulation. We may say that there are at least two different time scales in $I_s(Q, t)$. The effect of temperature on $I_s(Q, t)$ is seen in figure 4(*b*) where we show, for the same values of the triplet (n_1, n_2, n_3), the computed $I_s(Q, t)$ for the two temperatures considered. The $I(Q, t)$ is computed as

$$I(Q, \tau) = \frac{1}{N} \sum_{i=1}^{N} \frac{1}{\tau_{max}} \sum_{\tau_0=1}^{\tau_{max}} \frac{1}{nt} \sum_{j=1}^{nt} \rho_{n_{1j}, n_{2j}, n_{3j}}(\tau + \tau_0) \rho_{n_{1j}, n_{2j}, n_{3j}}(\tau_0) \qquad (15)$$

where

$$\rho_{n_{1j}, n_{2j}, n_{3j}}(\tau_0) = \sum_{i=1}^{N} \exp\left[\frac{i2\pi}{L}(n_{1j}, n_{2j}, n_{3j})\, r_i(\tau_0)\right].$$

This quantity is computed with time intervals of 0.02 ps for $T = 260$ K and $\Delta t = 0.025$ ps for $T = 293$ K and has been drawn in figure 5(*a*) for the three smallest values of the momentum transfer corresponding to the 293 K simulation. The figure at low Q resembles the one obtained by McDonald [10], i.e. an oscillation appears and we expect to have a phonon excitation (see also figure 5(*b*)). The modelling of $I(Q, t)$ and the study of collective excitation has been the subject of a subsequent paper [14].

The $I(Q, t)$ verifies [15]

$$\lim_{\substack{Q \to 0 \\ t \to 0}} I(Q, t) = \lim_{Q \to 0} S(Q) = \chi^* \rho / \beta$$

where χ is the isothermal compressibility that is equal to $8.31 \times 10^{-10}\ m^2\ N^{-1}$, $\beta = 1/k_B T$ and $\rho = N/V$ is the density.

All these correlation functions serve to analyse the translational motions. To investigate the rotational motion we have calculated the velocity autocorrelation function and the rotational relaxation functions $F_1(t)$ and $F_2(t)$.

3.5. Angular velocity autocorrelation function (AVACF)

This function comprises the details of the rotational motion of molecules in liquids and is calculated from

$$C(\tau) = \frac{\langle \boldsymbol{\omega}(t) \cdot \boldsymbol{\omega}(0) \rangle}{\langle \boldsymbol{\omega}(0) \cdot \boldsymbol{\omega}(0) \rangle} = \frac{1}{\omega_0^2} \frac{1}{N} \sum_{i=1}^{N} \frac{1}{\tau_{\max}} \sum_{\tau_0=1}^{\tau_{\max}} \boldsymbol{\omega}_i(\tau + \tau_0) \cdot \boldsymbol{\omega}_i(\tau_0). \tag{16}$$

The $C(\tau)$ functions for $T = 260$ K and $T = 293$ K are shown in figure 2(*b*).

There is a close similarity between the linear and angular velocity functions, at least at short times, suggesting that the same processes contribute to the randomization of both kinds of motion. This feature was noted by Lyndell-Bell [16] for tetrahedral molecules. As in the VACF, a negative overshoot appears in AVACF. It is caused by non-zero probability that during an interaction a molecule simply reverses its direction of rotation. Thus, the AVACF cannot be represented by a *J*-diffusion model in which the magnitude and the direction of the angular velocity is randomized at each collision [17]. We define a correlation time τ_ω by

$$\tau_\omega = \left[\int_0^\infty \langle \boldsymbol{\omega}(t) \cdot \boldsymbol{\omega}(0) \rangle \, \mathrm{d}t \right] \Big/ \langle \boldsymbol{\omega}(0)^2 \rangle \tag{17}$$

which gives $\tau_\omega = 0.13$ ps and 0.16 ps for $T = 260$ and 293 K respectively.

Since the AVACF cannot be represented by a simple exponential, therefore τ_ω cannot be simply related to a decay time.

3.6. First and second rotational relaxation functions

As we have pointed out before (see section 2) all the details of the dynamics of molecular reorientations relevant for cold neutrons experiments are $F_1(t)$ and $F_2(t)$. These quantities are calculated as follows

$$F_1(\tau) = \frac{1}{N} \sum_{i=1}^{N} \langle \boldsymbol{u}_i(t) \cdot \boldsymbol{u}_i(0) \rangle = \frac{1}{N} \sum_{i=1}^{N} \frac{1}{\tau_m} \sum_{\tau_0=1}^{\tau_m} \boldsymbol{u}_i(\tau + \tau_0) \cdot \boldsymbol{u}_i(\tau_0) \tag{18}$$

$$F_2(\tau) = \frac{1}{N} \sum_{i=1}^{N} \langle \tfrac{1}{2}[3(\boldsymbol{u}_i(t) \cdot \boldsymbol{u}_i(0))^2 - 1] \rangle = \frac{1}{N} \sum_{i=1}^{N} \frac{1}{\tau_m} \sum_{\tau_0=1}^{\tau_m} \tfrac{1}{2}[3(\boldsymbol{u}_i(\tau + \tau_0) \cdot \boldsymbol{u}_i(\tau_0))^2 - 1] \tag{19}$$

and are presented in figure 6(*a*) for $T = 260$ and 293 K respectively.

The relaxation times τ_1 and τ_2 may be obtained either from the slope of the logarithmic plots of $F_l(t)$ or from the integral

$$\tau_l^{\mathrm{int}} = \int_0^\infty \mathrm{d}t \, F_l(t). \tag{20}$$

If the $F_l(t)$ were exponentials, both definitions would agree. As this is not the case for our $F_l(t)$ curves, we have calculated the last integral on the best function that fits $F_l(t)$.

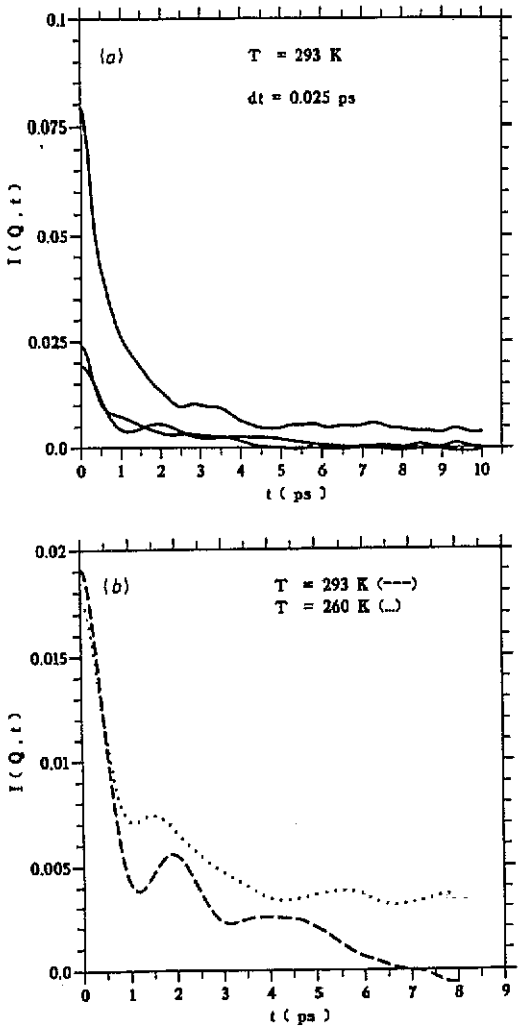

Figure 5. (*a*) Coherent intermediate scattering function $I(Q, t)$ at 293 K for the three lowest values of Q, 0.24291, 0.42074 and 0.80565 Å^{-1}; (*b*) $I(Q, t)$ for the lowest value of momentum transfer accessible at $T = 260$ K (dotted curve) and $T = 293$ K (broken curve).

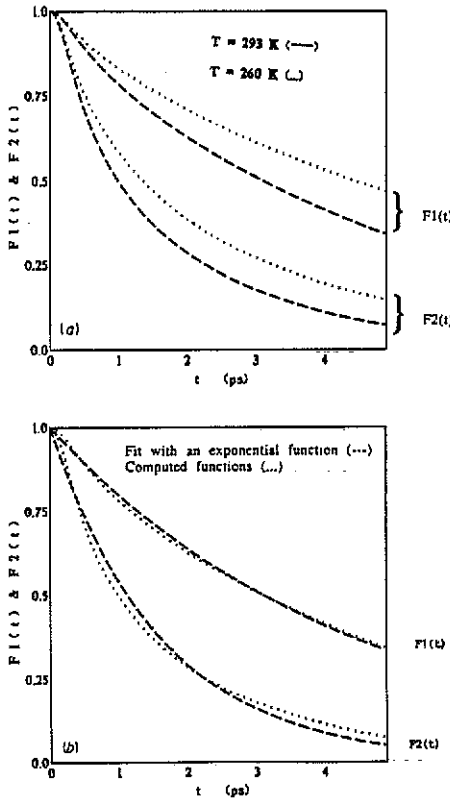

Figure 6. (*a*) First and second rotational relaxation functions at 260 (dotted curve) and 293 K (broken curve); (*b*) fit of these two functions (dotted curve) with an exponential function (broken curve).

Table 3. Values of τ_1 and τ_2.

	τ_1 (ps)	τ_2 (ps)
$T = 260$ K	6.554	2.344
$T = 293$ K	4.374	1.689

The integral was calculated at large times such that $F_l(t)$ goes to zero. The values obtained are summarized in table 3.

The experimental values for τ_2 determined by NMR [18] and Raman [19] measurements are $\tau_2 = 1.7$ ps and $\tau_2 = 1.8$ ps respectively at 296 K. The agreement is really as good as that of the diffusion constant.

4. Experimental results

The experiments were performed on the backscattering instrument IN13 at the Institut Laue–Langevin Grenoble [6]. This spectrometer has a good energy resolution—of the order of a few μeV—and covers a large range of the reciprocal space ($0.3\ \text{Å}^{-1} < Q < 5.5\ \text{Å}^{-1}$). A run at 275 K was carried out with a wavelength of 2.23 Å. The quasi-elastic contributions arise from coherent and incoherent effects and can be expressed by (4), i.e.:

$$u^2(Q)S_{\text{coh}}(Q, \omega) + v^2(Q)S_{\text{inc}}(Q, \omega).$$

In order to fit the experimental data we have used a simple Lorentzian function for the incoherent part, i.e.

$$S_{\text{inc}}(Q, \omega) = \Gamma/(\Gamma^2 + \omega^2)/\pi. \tag{21}$$

and we have used the Skold approximation to derive the coherent part, i.e.

$$S_{\text{coh}}(Q, \omega) = \Gamma^*/(\Gamma^{*2} + \omega^2)/\pi \qquad \text{where } \Gamma^* = \Gamma/S(Q). \tag{22}$$

The fits are good, as is shown in figure 7. We note that for low Q, the incoherent part is important whereas the coherent one is important at high Q. Since the energy window employed in this instrument is of about 0.02 meV, no information about the rotational dynamics can be obtained. However, the measurement enables one to obtain an estimate for the self-diffusion coefficient as well as the measurement of coherent effects at this frequency scale. From the slope of the curve giving the incoherent linewidth versus Q^2 a diffusion coefficient of $0.35 \times 10^{-5}\ \text{cm}^2\ \text{s}^{-1}$ has been computed.

It is difficult to follow the incoherent component at large Q-values since the value of the molecular form-factors given in (5) become very small for large values of the argument (Qa_{Cl}). As a consequence, the experimental spectra only show a measurable intensity in the wavevector range $0.3 < Q < 1.5\ \text{Å}^{-1}$. Therefore, the main result from this experiment is obtaining an estimate of the value of the self-diffusion coefficient. On the other hand the dependence on Q of the coherent linewidth has been given in a previous work [2].

5. Models

5.1. Models for the centre of mass motions

Although the quantities computed from the analysis of the classical trajectories encompass all the sought information, they are of scarce use when trying to understand the nature of the underlying physical processes which drive the microscopic thermal motion of the fluid. On the other hand it is clear that the above quantities are of small use when confronted with the task of analysing the experimental intensities. For such a

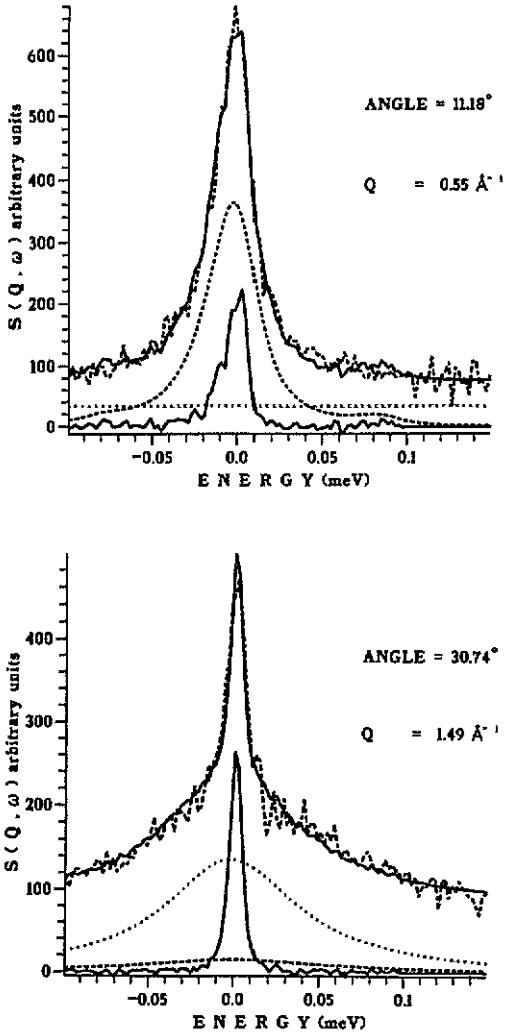

Figure 7. Fit of the experimental data obtained on IN13 by a function of the form (3). The full curve under the experimental point represents the resolution. At low Q, the incoherent part (broken curve) is important whereas the coherent one (dotted curve) is important at large Q.

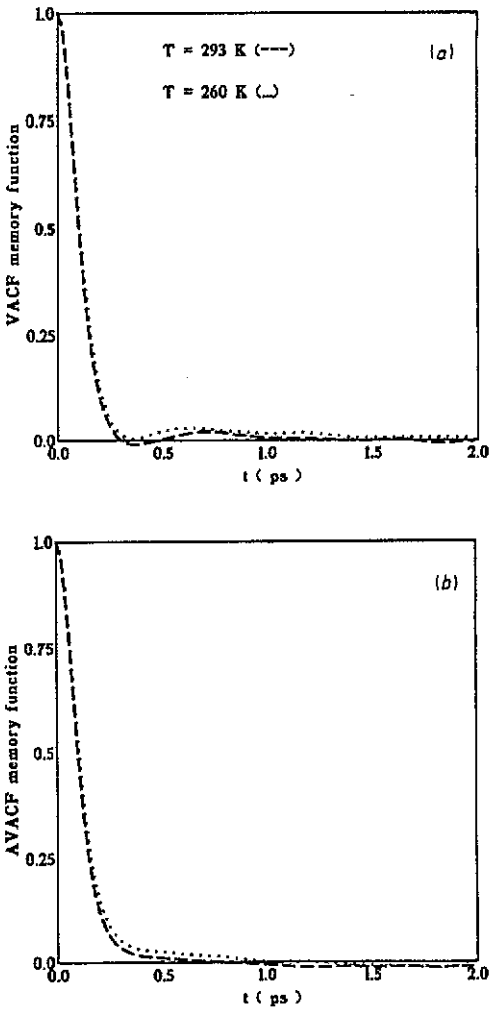

Figure 8. Memory function (MF) of the VACF (a) and of the AVACF (b) at the two temperatures considered.

purpose, the most convenient way of extracting the rich information contained in the simulation is constituted by the analysis in terms of dynamical models which will serve to express the complicated time and wavevector dependences shown by the computed autocorrelation functions in terms of simpler counterparts. From an experimental point of view, the aim of such an exercise is to derive easily parametrizable functions able to describe the pertinent kind of motion in terms of a few relaxational processes, so that, at some stage, they could serve as a tool for spectral analysis in order to obtain, from comparison with the experiment, the relaxation times and amplitudes.

The important quantity relevant to the analysis of the VACF is $K(t)$, the memory function of $\psi(t)$ that is computed by solving the memory equation [20, 21]:

$$\frac{d\psi(t)}{d\tau} = -\int_0^t K(t-\tau)\psi(\tau)\,d\tau. \tag{23}$$

The motivation for the use of memory functions is based on the hope that a possibly complicated correlation function $\psi(t)$ can be generated through (23) by a simpler (more easily parametrizable) function $K(t)$.

For very short times the tagged particle creates a perturbation in the fluid that propagates in time and influences the force on the particle at time t. This retardation effect, neglected in the simple Langevin equation, is described by the generalized Langevin equation where the concept of memory function is introduced. $K(t)$ is shown in figure 8(a) for the two temperatures considered. It contains a rapidly decaying component which reflects the effects of individual interaction between the tagged molecule and its neighbours.

A particularly useful extension of the last equation has been developed by Mori [22, 23], who assumed the set of kernels $K_0(t), \ldots, K_n(t)$ to obey the set of coupled Volterra equations such that

$$\frac{\partial K_{n-1}(t)}{\partial t} = -\int_0^t K_n(t-\tau)K_{n-1}(\tau)\,d\tau \tag{24}$$

with $n = 1, \ldots, N$. Taking the Laplace transform,

$$C(p) = C(0)/[p + K_0(p)] = C(0)/\{p + K_0(p)/[p + K_1(p)]\} = \ldots \tag{25}$$

which is a continued fraction approximation to the function $C(p)$.

Many authors truncate this hierarchy at zero-order assuming $K_0(t)$ to have an exponential or Gaussian form. They obtain results which sometimes are not in good agreement with experiments but if the hierarchy is truncated at the first order, then the agreement between postulated and exact correlation functions is satisfactory.

In our case the fit with an exponential or a Gaussian function of the memory function calculated from (23) gives rather poor fits at short time and does not reproduce the main minimum (see figure 9). So we have calculated the memory function $K_1(t)$ from (24) and then we have tested some function $y(t)$ that verifies,

$$K_1(t) = K_1(0)y(t). \tag{26}$$

If we take for $y(t)$ an exponential, it is easy to derive an algebraic expression for the velocity correlation function which results [24],

$$\psi(t) = \{(\cos(\beta t)/1 + \Gamma) + (1/\beta)[(\alpha_1 + \Gamma\alpha_2)/(1 + \Gamma)]\sin(\beta t)\}\exp(-\alpha_1 t) + [\Gamma/(1 + I)]\exp(-\alpha_2 t) \tag{27}$$

where

$$\Gamma = [2\alpha_1(2\beta^2 - \alpha_1^2)]/[\alpha_2(3\alpha_1^2 - \beta^2 - \alpha_2^2)].$$

It is shown in figure 10 that this function gives good fits to the computed $\psi(t)$ at short times. At large times (from 0.4 ps) a large deviation from the computed curve is observed.

To measure the accuracy of the various models $K_1^m(t)$ proposed for the computed

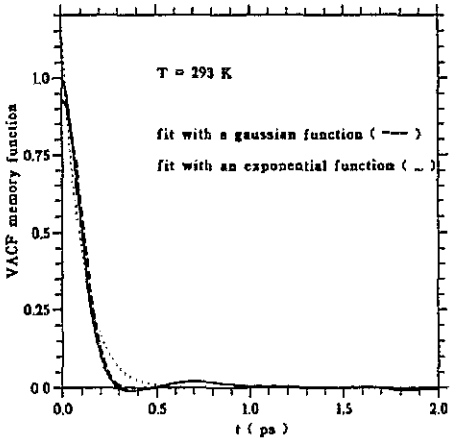

Figure 9. Fit of the MF of the VACF at 293 K with a Gaussian and with an exponential function. The figure shows that this MF is nearer a Gaussian than an exponential form.

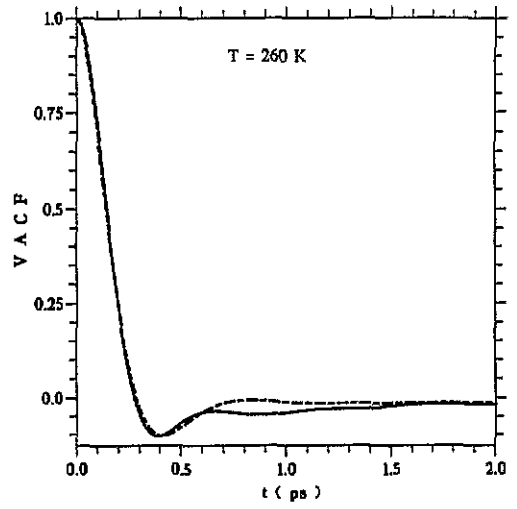

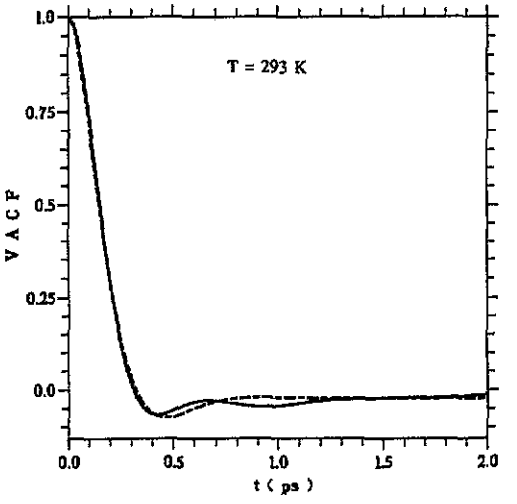

Figure 10. Fit of the MF of the VACF at 260 K and 290 K (solid curve) with a function of the form (27) (broken curve), see text.

$K_1^s(t)$ we show in table 4 the results of a chi-square statistic test for the set of models explored [25]:

We see from this table that the 2G model gives the best fit for both the VACF and the AVACF.

5.1.1. $I_s(Q, t)$. Any suitable model to fit the computed data of $I_s(Q, t)$ should have the correct limits in the long and short (t, λ) space. These asymptotic limits correspond to diffusion and to free particle regimes, respectively. The first model we have tested is the one proposed by Egelstaff–Schofield [26] which has been used in [2] to fit experimental data. Poor fits were obtained, so that it was not possible to estimate a reasonable friction

Table 4. Chi-square statistic test for a set of models explored to reproduce the $K_1(t)$ memory function.

		$\chi^2 10^4$			
		VACF		AVACF	
	Functions used	260 K	293 K	260 K	293 K
1G	$\exp[-(t/t_1)^2]$	1.331	3.426	0.939	2.777
2G	$(1-c)\exp[-(t/t_1)^2] + c\exp[-(t/t_2)^2]$	1.326	0.336	0.910	0.374
G + t^2E	$\exp[-(t/t_1)^2] + ct^2\exp[-(t/t_2)]$	1.340	3.463	0.946	2.861
1EXBIN	$(1 + t/t_1)\exp[-(t/t_1)]$	3.720	5.705	3.575	6.191
2EXBIN	$(1-c)(1 + t/t_1)\exp[-(t/t_1)] + c(1 + t/t_2)\exp[-(t/t_2)]$	1.483	3.844	1.174	3.407

constant. A second model based on the Gaussian approximation satisfies the low and large Q limit but it is not adequate for intermediate values of Q. In order to improve it, we have taken into account the first non-Gaussian correction in the expansion of $I_s(Q, t)$, i.e.,

$$\alpha(t) = 3\langle r^4\rangle/5\langle r^2\rangle^2. \tag{28}$$

Levesque and Verlet [13] have fitted this quantity and have obtained the following form for $I_s(Q, t)$:

$$I_s(Q, t) = \exp(-(1/6)Q^2\langle r^2(t)\rangle)\,[1 + [Q^4\langle r^2(t)\rangle/72]C(t_c/t)\exp - ((t_c/t) - 1)]. \tag{29}$$

We have used for $\langle r^2\rangle$ either the computed value or a fit of this with an itinerant oscillator model [27]. The fits obtained were quite good and gave the following values for C and t_c:

0.0601 and 3.568 ps for 260 K and

0.0947 and 2.832 ps for 293 K.

In figure 11(b) we have plotted the incoherent HWHM versus Q^2 deduced from the fit of $I_s(Q, t)$ by a sum of two exponential functions which take into account the two time scales of $I_s(Q, t)$.

5.2. *Models for rotation*

5.2.1. $\langle\omega(t)\omega(0)\rangle$. This function has the same form as $\psi(t)$, so we have used the same procedure as for the VACF. As shown in figure 12, this function is well fitted at short time by a function of the form (27). Good fits are also obtained with the 2G model for $K_1(t)$ corresponding to this function.

5.2.2. $F_l(t)$. As a first approximation, we take a simple rotation diffusion model for $F_l(t)$; i.e.

$$F_l(t) = \exp[-l(l + 1)D_r t] \tag{30}$$

where D_r is the rotational diffusion constant. One can see from figure 6(b) that $F_1(t)$ is more closely approximated to an exponential than $F_2(t)$. Although the value of D_r obtained by the fit (0.1024 ps^{-1}) agrees with the one deduced from NMR measurements by the relation $\tau_{NMR} = 1/6D_r$ (0.0981 ps^{-1}), the fits are rather poor and we can conclude

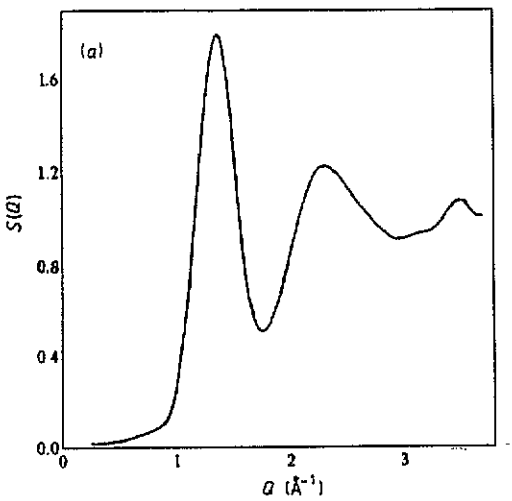

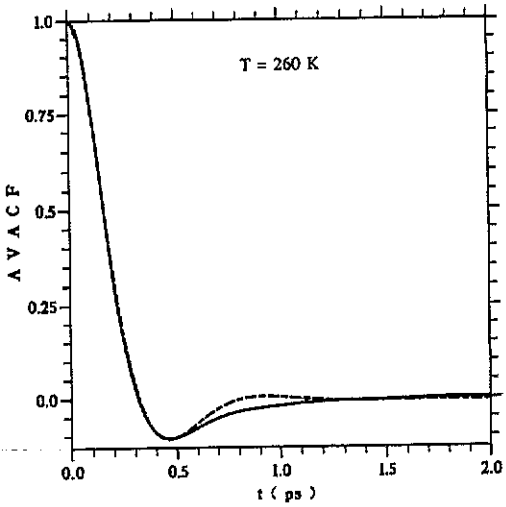

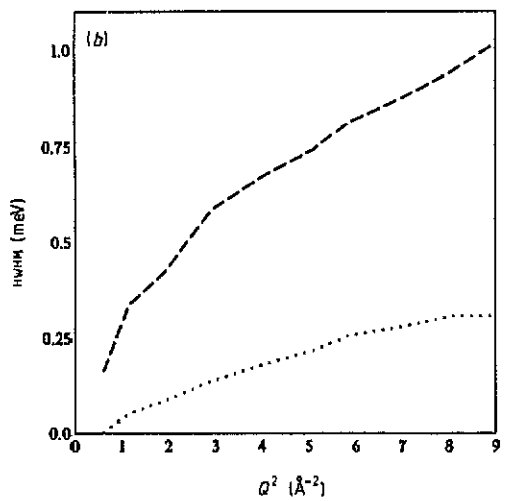

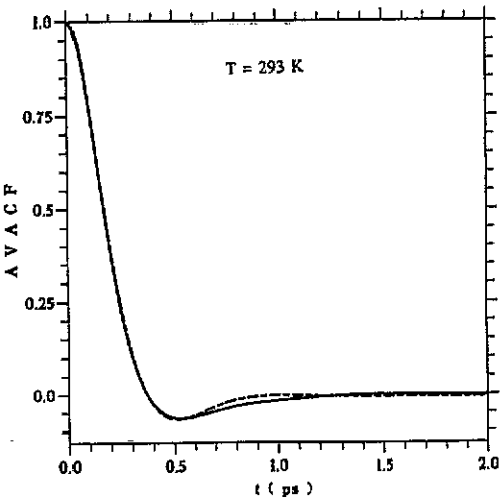

Figure 11. (*a*) Structure factor $S(Q)$ obtained from the simulation at 293 K; (*b*) HWHM of the incoherent simulated part.

Figure 12. Fit of the MF of the AVACF at 260 K and 293 K (solid curve) with a function of the form (27) (broken curve), see text.

that the rotational–diffusion model is only approximately valid for CCl_4 as has been pointed by Steinhausser [28]. The model that adequately reproduces the $F_1(t)$ is the one used by Levesque [29]. The ingredients of this model are a sum of a Gaussian function that reproduces the fast decay at short time $t < 4$ ps, and an exponential function that reproduces the decay for $t > 4$ ps. This model is given by

$$a_1 \exp(-a_2 t^2) + a_3 \exp(-a_4 t) + (1 - a_1 - a_3) \exp(-a_5 t). \tag{31}$$

For large times the term proportional to $\exp(-a_4 t)$ is dominant whereas for short times the Gaussian term is dominant. The exponential term $\exp(-a_5 t)$ is added only to ensure that at short times no linear term is present in the expansion of $F_1(t)$. The fits, as well as the relevant parameter values, are given in figure 13.

6. Conclusion

The aim of the present work was to explore the fine details of the single-particle dynamics of liquid carbon tetrachloride in order to overcome some difficulties encountered when analysing the quasi-elastic spectra. Since all the relevant quantities entering in (1) have been calculated, it becomes natural to compute the total dynamical structure factor $S_{tot}(Q, \omega)$. This is done for two values of the momentum transfer with the measured spectra described in [2]. Such a comparison is presented in figure 14. As can be easily

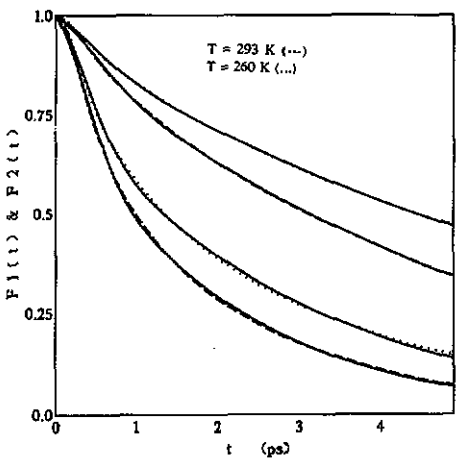

		a_1	a_2	a_3	a_4	a_5
260 K	F_1	0.050	1.946	1.312	0.145	0.145
	F_2	0.192	2.984	0.931	0.360	0.364
293 K	F_1	0.089	1.549	3.722	0.287	0.325
	F_2	0.239	2.905	2.148	0.562	0.614

Figure 13. Fit of the rotational relaxation function with a Levesque function: (31) (see text).

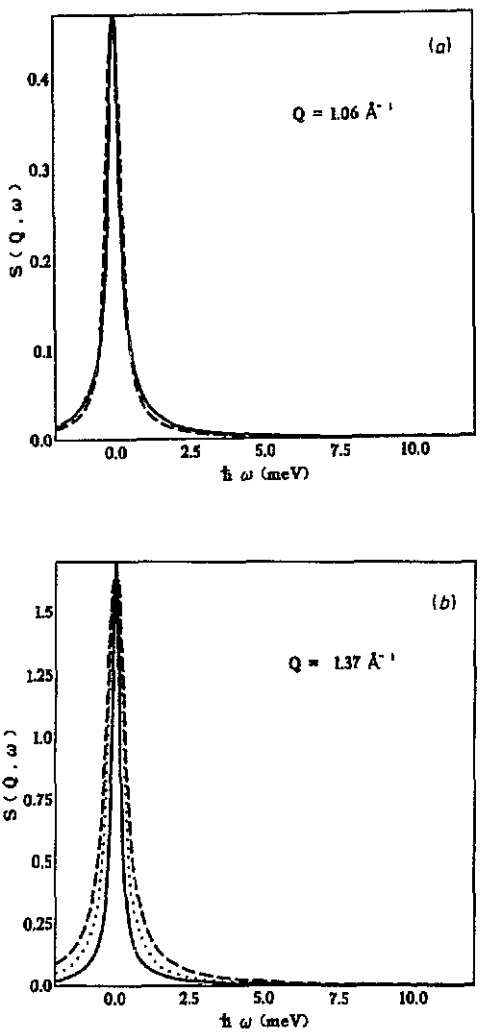

Figure 14. (*a*) Calculated $S(Q, \omega)$ with uncorrelated orientation (broken curve) and experimental (solid curve) $S(Q, \omega)$ for a momentum transfer of 1.06 Å^{-1}. (*b*) Calculated $S(Q, \omega)$ with uncorrelated orientation (broken curve), and with correlated orientation (dotted curve) and experimental one (solid curve) for $Q = 1.37$ Å^{-1}.

seen, the approximation given by (1) which assumes that the molecular orientations are uncorrelated gives a reasonable account of the lineshape for momentum transfers not situated in the vicinity of the maximum of the peak in $S(Q)(Q_p)$. However such approximation breaks down at Q_p where the calculated width is about double the experimental one. A way of improving it is to modify the orientational factor $F(Q)$ in order to take into account the strong correlations at short distances. For such a purpose we have used for this quantity the approximation described in [30] which gives

$$F(Q) = b_C^2 + 8b_C b_{Cl}[\sin(Qr_{C\text{-}Cl})/Qr_{C\text{-}Cl}] + b_{Cl}^2 + 6b_{Cl}^2[(\sin(Qr_{Cl\text{-}Cl}))/Qr_{Cl\text{-}Cl}] + 9b_{Cl}^2 I(Qr_t) \tag{32}$$

where

$$I(Qr_t) = \int_0^{\pi/2} J_0^2(Qr_t \sin(\theta)) \sin(\theta)\, d\theta \tag{33}$$

and $r_t = r_{C\text{-}Cl} \sin(\pi - \theta)$; where θ is the tetrahedral angle.

The computed lineshape in figure 14(*b*) is now closer to the experimental one although it still shows a significant deviation. It seems difficult to reconcile this difference unless a model which explicitly takes into account the coupling between translation and rotation similar to the one described in [31] is used. On the other hand it becomes clear that, in order to reconcile this deviation one has to take explicitly into account in (1) the effects of low-energy collective phenomena such as cooperative molecular reorientations or some kind of collective interplay between molecular linear and angular motions. This is quite a considerable task and, up to the present moment only the preliminary blocks of a theory able to predict the influence of the effects on the measured neutron cross-sections have been reported (see, for instance, [32]).

In summary, for such a simple molecular liquid it has been found that (a) in a way closely resembling the case of liquefied rare-gases, the translational correlation functions can be adequately described in terms of a Gaussian approximation corrected up to a first order; (b) the rotational motion evidences a clear departure from simple diffusional behaviour as has been noted previously from NMR [19] and quasi-elastic neutron scattering experiments [2]. An empirical model consistent in a sum of Gaussian and exponential functions has been proven to give a reasonable account of the rotational relaxation functions, and the obtained τ_2 correlation times are in good agreement with those determined from NMR relaxation; (c) the obtained diffusion coefficients are in good agreement with those determined by either tracer diffusion or from the Q dependence of the inelastic incoherent linewidths.

Finally, it is worth recalling the fact that it is only in such a relatively simple molecular liquid that noticeable departures from idealized rotational behaviour can be seen, whereas most of the data regarding complex fluids (i.e. associated liquids) are still accounted for in terms of such simple models. The observed departures from simple rotational diffusion are, in our case, rather puzzling if one takes into account the relatively large molecular mass as well as the conventional picture of its liquid structure which portrays it as consisting of closely interlocked molecular units.

The simple character of this liquid has also been noted in a recent study of its collective dynamics [14] where the observed excitations are of an overdamped nature in most of the explored Q-range and the contribution of thermal (and collisional) mechanisms to the observed coherent response are rather large in comparison with structural relaxation effects dominant in more complex fluids.

To end with, the present work emphasizes the need of a concurrent use of simulation techniques together with QENS measurements in order to exploit fully the information obtainable from experimental means.

Acknowledgments

Work supported in part by DGICYT (Spain) grant No PB89-0037-C03. A Chahid acknowledges the receipt of a post-doctoral grant from DGICYT (Spain). It is a pleasure to thank the Science and Engineering Research Council (UK) CCP5 group for access to their library.

References

[1] Bermejo F J, Enciso E, Alonso J, Garcia N and Howells W S 1988 *Mol. Phys.* **64** 1169
[2] Bermejo F J, Alvarez M, Garcia M, Mompean F, White R P, Carlile C J and Howells W S 1991 *J. Phys.: Condens. Matter* **3** 851; 1990 *J. Phys.: Condens. Matter* **2** 1301
[3] Bermejo F J 1991 *Proc. Ann. Mtg American Cryst. Assoc. (Toledo, OH); Physica* B at press
[4] Venkataram G, Dasannacharya B A and Rao K R 1967 *Phys. Rev.* **161** 1
[5] Sears V F 1966 *Can. J. Phys.* **44** 1299
[6] Blank H and Maier B (ed) 1988 *Guide to Neutron Research Facilities at the ILL* Grenoble, France
[7] Yip S 1974 Quasi-elastic scattering in neutron and laser spectroscopy *Spectroscopy in Biology and Chemistry: Neutrons, X-Rays, Laser* ed S H Chen and S Yip (New York: Academic) ch 2
[8] Gordon R G 1968 *Advances in Magnetic Resonance* vol 3, ed J S Wangh (New York: Academic) p 1
[9] Thompson S M 1985 Program 'MDTETRA', from CCP5 Program Library, Daresbury Laboratory
[10] McDonald I R, Bounds D G and Klein M L 1982 *Mol. Phys.* **45** 512
[11] Rothschild W G 1984 *Dynamics of Molecular Liquids* (New York: Wiley) p 172
[12] Zwanzig R and Ailawadi K A 1969 *Phys. Rev.* **182** 280
[13] Levesque D and Verlet L 1970 *Phys. Rev.* A **2** 2514
[14] Garcia-Hernandez M, Martinez J L, Bermejo F J, Chahid A and Enciso E 1991 *J. Chem. Phys.* submitted
[15] Lovesey S W 1986 *Theory of Neutron Scattering from Condensed Matter* (Oxford: Oxford University Press) p 172
[16] Lyndell-Bell R M and McDonald I R 1981 *Mol. Phys.* **43** 1429
[17] Gordon R G 1966 *J. Chem. Phys.* **44** 1830
[18] O'Reilly D E and Schacher G E 1968 *J. Chem. Phys.* **39** 1963
[19] Bartoli F J and Litovitz T A 1972 *J. Chem. Phys.* **56** 413
[20] Boon J P and Yip S 1982 *Molecular Hydrodynamics* (New York: McGraw-Hill) p 70
[21] Hoheisel C 1990 *Comput. Phys. Rep.* **12** 29
[22] Mori H 1965 *Prog. Theor. Phys.* **33** 423
[23] Berne B S and Harp J D 1970 *Adv. Chem. Phys.* **17** 63
[24] Davies G J and Evans M 1975 *J. Chem. Soc. Faraday Trans.* II **72** 1194
[25] Detyna E, Singer K, Singer J V L and Taylor A J 1980 *Mol. Phys.* **41** 31
[26] Egelstaff P A 1976 *An Introduction to the Liquid State* (New York: Academic) p 129
[27] Sears V F 1965 *Proc. Phys. Soc.* **86** 953
[28] Steinhausser O and Neumann D 1980 *Mol. Phys.* **40** 115
[29] Levesque D and Weis J J 1975 *Phys. Rev.* A **12** 2584
[30] Egelstaff P A, Page D I and Powles J G 1971 *Mol. Phys.* **20** 881
[31] Davies A R, Evans G J and Evans M W 1978 *Faraday Discuss.* 66/15, 1A
[32] Chandra A and Bagchi B 1990 *Physica* A **169** 246
Deb S K 1988 *Chem. Phys.* **120** 225